Journal of Inorganic and Organometallic Polymers and Materials (2023) 33:398–406
https://doi.org/10.1007/s10904-022-02507-6

RESEARCH

Controlled Chemical Transformation and Crystallization Design for the Formation of Multifunctional Cu-Doped ZnO/$ZnAl_2O_4$ Composites

Artiom Tincu[1] · Andrey Aleksandrovich Shelemanov[1] · Sergey Konstantinovich Evstropiev[1,2,3] · Nikolay Valentinovich Nikonorov[1] · Konstantin Vladimirovich Dukelskii[1,2,4]

Received: 28 September 2022 / Accepted: 26 October 2022 / Published online: 9 November 2022

Graphical Abstract

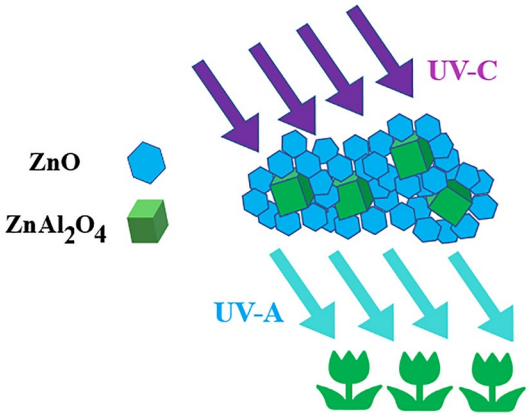

Keywords Nanocrystals · Luminescence · ZnO · $ZnAl_2O_4$ · Singlet oxygen

1 Introduction

It is well known that materials based on zinc oxide are one of the most effective among oxide photocatalysts and bactericidal solids [1–5]. ZnO-based heterostructural composites containing various semiconductor and metal nanoparticles, are especially effective [5–10].

✉ Andrey Aleksandrovich Shelemanov
shelemanov@mail.ru

1 ITMO University, Saint-Petersburg, Russia

2 Saint-Petersburg State Technological Institute (Technical University), Saint Petersburg, Russia

3 RPA "Vavilov State Optical Institute", Saint-Petersburg, Russia

4 The Bonch-Bruevich Saint-Petersburg State University of Telecommunications, Saint-Petersburg, Russia

Cu-containing ZnO–Al_2O_3 nanocomposites demonstrate high photocatalytic and bactericidal properties and are considered also as effective catalyst for reforming CO_2 to different organic compounds, photoactive and luminescent materials, and potential candidates for sensors applications [11–20]. It was established in [12] that ZnO nanomaterials doped with copper exhibit good antibacterial activity, which increases with increasing level of copper doping.

The generation of reactive oxygen species (singlet oxygen [17, 21–23], superoxide radicals [24, 25], hydroxyl radical [21, 24]) plays the key role in photocatalytic processes and materials bactericidal activity [21–24]. Characteristics of exciting radiation, electronic structure, and morphology of materials affect the efficiency of their photogeneration [21–24, 26, 27].

The highly dispersive materials, consisting of small nanoparticles with high surface area, show higher photocatalytic properties and antibacterial activity

compared with macroscopic ones [27]. The decrease of the size of photoactive particles and the optimization of materials morphology are used for the enhancement of their photocatalytic and bactericidal efficiency [22, 23, 28–31]. It is known [22, 23, 32] that the sizes of crystals in two-component oxide composites are smaller than in one-component analogs obtained by the same method under similar technological conditions. In [17, 22, 23] this approach was used for the fabrication of highly dispersive photoactive materials ZnO–Al_2O_3 [17], ZnO–SnO_2 [22] and ZnO–MgO–Ag [23].

Different methods have been applied for the preparation of Cu-containing ZnO nanomaterials: glucothermal method [7], co-precipitation [11, 15], polymer-salt [16], etc. Polymer-salt method based on the application of initial solutions containing metals salts and soluble organic polymers is widely used for the preparation of different materials [9, 10, 17–19, 22, 23]. The temperature–time schemes of technological processes used in [17, 22, 23] provide the simultaneous formation of different crystals (ZnO + γAl_2O_3 [17], ZnO + SnO_2 [22] and ZnO + MgO [23]) without their chemical interaction. The simultaneous formation of different crystals prohibits their growth and the aggregation and provides the formation of the material structure consisting of small particles with high specific surface area.

Photocatalytic and bactericidal properties of ZnO are well-known [28–30, 33, 34]. Also, the application of $ZnAl_2O_4$ nanoparticles as photocatalytic material was studied in [4–7, 35–40]. The literature data about $ZnAl_2O_4$ band gap value vary from ~ 3.9 eV to more than 6.0 eV [9, 41–43]. Cu additions can improve photocatalytic characteristics of $ZnAl_2O_4$ [11].

The aim of this work was to synthesis of Cu-doped ZnO–$ZnAl_2O_4$ nanocomposites which can be used as luminescent spectral down-converters and bactericidal materials by the polymer-salt method and to study their structure, luminescent and bactericidal properties, and the ability to generate singlet oxygen.

2 Materials and Methods

The polymer-salt method which is applied for the synthesis of different nanoparticles [9, 10, 17–20] was used in this study. The aqueous solutions of $Zn(NO_3)_2$, $Al(NO_3)_3$ and $CuSO_4$ were used as raw materials for the nanocomposites synthesis. The solution of polyvinylpyrrolidone (PVP) (K30; M_w = 25,000–35,000) in propanol-2 was added to the mixture of aqueous solutions of metal salts. Obtained mixtures were stirred for 30 min at room temperature. After drying obtained polymer-salt composites were calcined in air atmosphere at 680 °C for 2 h. Chemical compositions of initial solutions and obtained composites are given in Table 1.

The diffractometer Rigaku Ultima IV was used for X-ray diffraction (XRD) analysis of prepared materials. The diffraction patterns were scanned from 20° to 100° (2θ). The crystallite size was calculated using the Scherrer's equation:

$$d = \frac{0.9\lambda}{\beta\cos\theta} \quad (1)$$

where $\boldsymbol{d}$ is the average grain size of the crystallites, $\boldsymbol{\lambda}$ the incident wavelength, $\boldsymbol{\theta}$ the Bragg angle (radians) and $\boldsymbol{\beta}$ is the full width at half maximum (FWHM) in radians.

The photoluminescence measurements were carried out on the Perkin Elmer LS-50B fluorescence spectrophotometer in the spectral range 200–650 nm.

To study the antibacterial activity of the oxide composites, the method based on the diffusion into agar and described in [44] was used. The test used representative of the gram-positive bacteria ***Staphylococcus aureus ATCC 209P***. The bactericidal activity was assessed by measuring the size of the inhibited zone. The experiments were carried out in natural light.

Table 1 Chemical composition of initial solutions and obtained composites

Sample	Chemical composition of solutions, wt%						Chemical composition of powders, mol.%		
	H_2O	PVP	Propanol-2	$Zn(NO_3)_2$ •$6H_2O$	$Al(NO_3)_3$ •$6H_2O$	$CuSO_4$· $5H_2O$	ZnO	$ZnAl_2O_4$	CuO[a]
1	51.6	2.58	40.6	3.38	1.77	0.013	78.90	20.65	0.45
2	51.6	2.58	40.6	3.82	1.33	0.014	85.86	13.71	0.43
3	51.6	2.58	40.6	4.09	1.07	0.015	89.23	10.34	0.43
4	51.6	2.58	40.6	4.27	0.9	0.015	91.28	8.33	0.39

[a]All Cu content was calculated in the form of CuO

Table 2 Average sizes and lattice parameters of ZnO crystals in nanocomposites

Sample	Average ZnO crystals size, nm	Lattice parameters of ZnO crystals			
		a (Å)	***c*** (Å)	c/a	V (Å^3)
1	25.1	3.2447(8)	5.1955(16)	1.6012	47.37(2)
2	14.1	3.2392(6)	5.1834(27)	1.6002	47.10(2)
3	8.2	3.2444(6)	5.1938(12)	1.6009	47.35(2)
4	14.6	3.2490(5)	5.1954(9)	1.5991	47.50(1)
ZnO[a]	–	3.2475–3.2501	5.2042–5.2075	1.593–1.6035	

[a]The data of the review of experimental values given in [3]

3 Crystal Structure

XRD patterns of all powders show the peaks characteristic for hexagonal ZnO crystals (JCPDS № 36-1451). The ratios between intensities of different ZnO peaks are close to standard values that indicates the absence of the texture in prepared materials. The lattice parameters of ZnO crystals and their average sizes obtained from XRD data is given in Table 2.

The structures of prepared composites consist of small nanocrystals. The average sizes of ZnO crystals are 8–25 nm that is less than the size of similar crystals in ZnO–MgO (32–35 nm, [45]) and ZnO–MgO–Ag (22–25 nm, [23]) powder composites previously formed by the similar polymer-salt technique at 550 °C. In addition, the size of ZnO crystals is close to that was observed in ZnO–$ZnAl_2O_4$ composites obtained by the sol–gel method at a temperature of 600 °C (19–22 nm) [16]. In [23, 45] MgO particles played the barrier role by spatially separating ZnO crystals and preventing their aggregation and the growth. Based on the presented experimental results, it can be concluded that limiting the growth of the formed ZnO crystals by chemical transformation of some of them into another crystalline matrix ($ZnAl_2O_4$) at the stage of crystallization of the material is also effective.

The lattice constants of hexagonal ZnO crystals mostly range from 3.2475 to 3.2501 Å for the ***a***-parameter and from 5.2042 to 5.2075 Å for the ***c***-parameter [3]. Cu^{2+} ions slightly smaller than Zn^{2+} (ionic radii 0.57 and 0.60 Å, correspondingly) and Cu^{2+} easily replace Zn^{2+} in crystal structure that leads to contraction of crystal cell [46]. Therefore, the absence of any peaks of Cu compounds (Fig. 1) and lower values of lattice parameters ***a*** and ***c*** of formed ZnO crystals compare with the literature data [3] (Table 2) may indicate the incorporation of copper ions into their structure. This corresponds to the data reported in [16] that ZnO–CuO materials with copper content lower than 15% are one-phase wurtzite-like $Cu_xZn_{1-x}O$.

The XRD patterns of all prepared samples show peaks related to cubic crystals of $ZnAl_2O_4$ (JCPDS No. 05-0669). This fact is agreed to the previous studies [9, 11, 47] that the application of different liquid-phase techniques (co-precipitation [11], sol–gel [20, 47], polymer-salt method [9], etc.) provides the formation of $ZnAl_2O_4$ crystals at relatively low temperatures (T > 550 °C [47]).

SEM analysis showed that the composites consist of nanoparticles with a size of < 20 nm (Fig. 2a) that can facilitate their effective contact with the environment and impart high photocatalytic and bactericidal characteristics to the materials. The morphology of the resulting composites is similar to that demonstrated in [9] for $ZnAl_2O_4$ xerogels. Observed nanoscale morphology of composites fully agrees to the data of their crystal structure obtained from XRD analysis.

4 Photoluminescence

Numerous emission peaks are observed in photoluminescence spectra of prepared powders (Fig. 2). These peaks are located at 343, 399, 423, 440, 461, 487 and 533 nm. Usually, two main emission bands are observed in luminescence spectra of ZnO-based materials: excitonic peak (NBE) in near UV region and wide emission band in visible spectral range that is related to different defects of ZnO crystal structure [48].

In the photoluminescence spectra of ZnO thin films obtained by radio frequency (RF) magnetron sputtering, many emission peaks were observed associated with the recombination of photogenerated holes with various structural defects, for example, ionized charge states of intrinsic defects, oxygen vacancies, zinc interstices, and zinc vacancies [2]. These luminescence bands were in ultraviolet (λ_{max} = 399 nm), violet (λ_{max} = 417, 438, 453 nm), blue (λ_{max} = 467 nm) and green spectral ranges.

Cu additions into ZnO crystal structure decrease the materials band gap value [16] and significantly increase the amount of emission peaks [1, 15]. Photoluminescence spectra of $CuO{\cdot}ZnO{\cdot}ZnAl_2O_4$ showed four peaks at 411, 433, 459 and 492 nm [15].

$ZnAl_2O_4$ crystals are considered as potential ultraviolet emitting phosphor for the medical sterilization lamps [49]. These crystals emit short-wave ultraviolet (UV-C) light under vacuum UV ($\lambda_{ex.}$ < 200 nm) irradiation with high

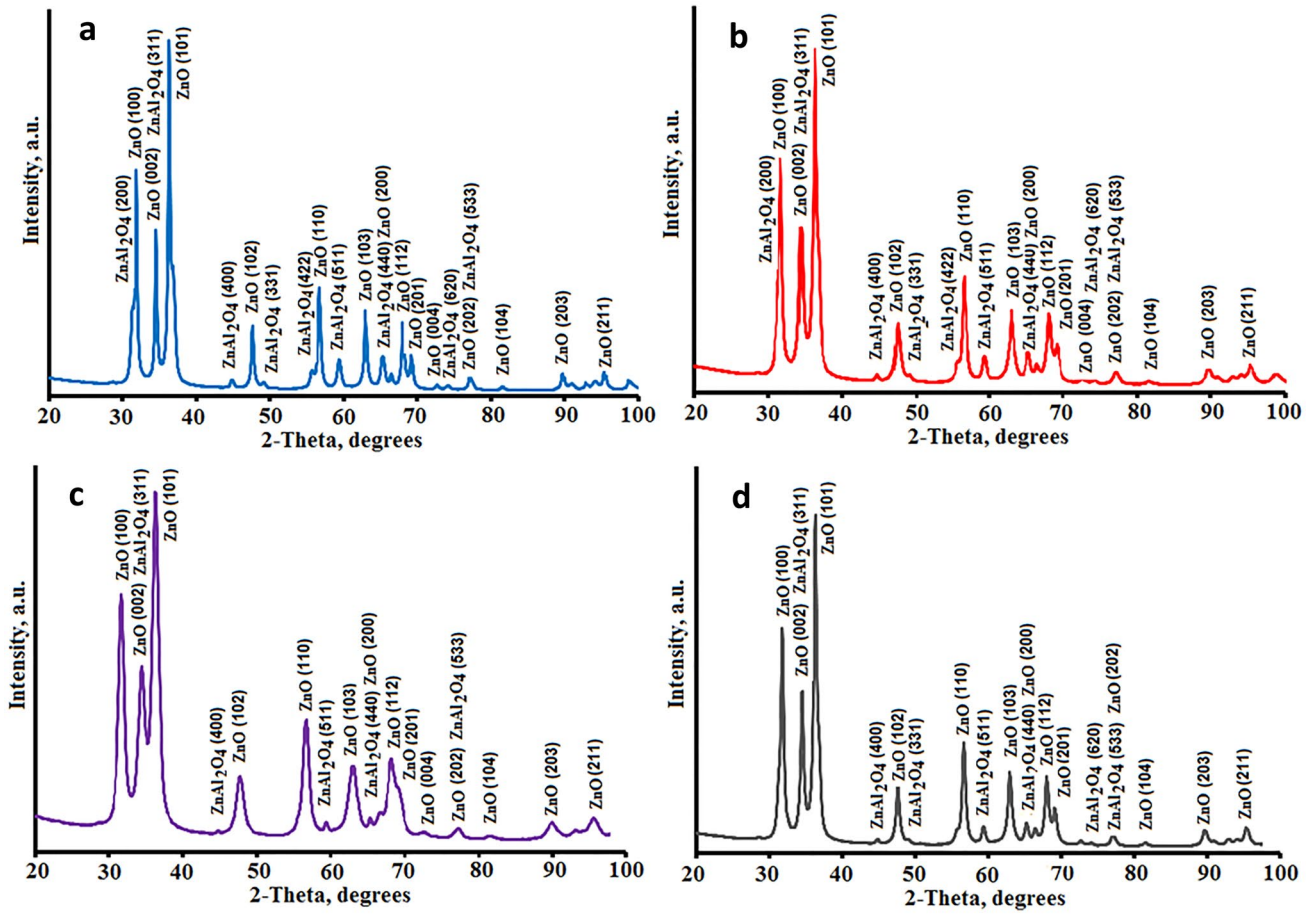

Fig. 1 XRD patterns of prepared powders with different Al_2O_3 contents. Samples ***1*** (**a**); ***2*** (**b**); ***3*** (**c**); ***4*** (**d**)

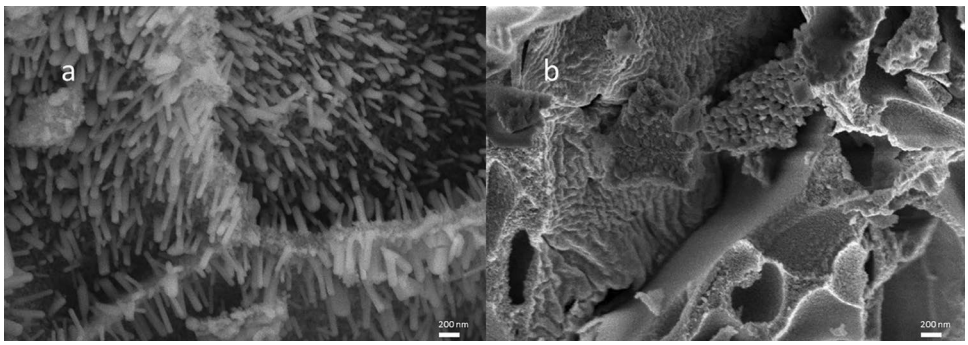

Fig. 2 SEM image of samples ***1*** (**a**) and ***3*** (**b**)

effectiveness [49]. Three emission bands with maximums at 400, 411 and 444 nm were observed in luminescence spectra ($\lambda_{ex.} = 325$ nm) of $ZnAl_2O_4$ nanoparticles prepared by polymer-salt method [9]. These emission peaks can be ascribed to intra band gap defects such as oxygen vacancies [9, 10]. The luminescence peaks located at 428 and 561 nm attributed to structural defects were observed in ZnAl2O4/ZnO composites obtained by citrate sol–gel method [16].

The peak located at ~ 340 nm (Fig. 3) can be assigned to the emission of $ZnAl_2O_4$ crystals. It is worth noticing that this emission is observed under UV irradiation ($\lambda_{ex.} = 240$ nm). So, obtained materials play the role of down-converters absorbing UV-C radiation and emitting the light of long-wave ultraviolet (UV-A) spectral range. Such down-converters can increase the efficiency of solar panels based on the ground and in space.

It is known that UV radiation can be divided into three parts: UV-A (320–400 nm), middle-wave ultraviolet (UV-B) (280–320 nm), and UV-C (200–280 nm). Because UV-C radiation has higher photon energy than the binding energy

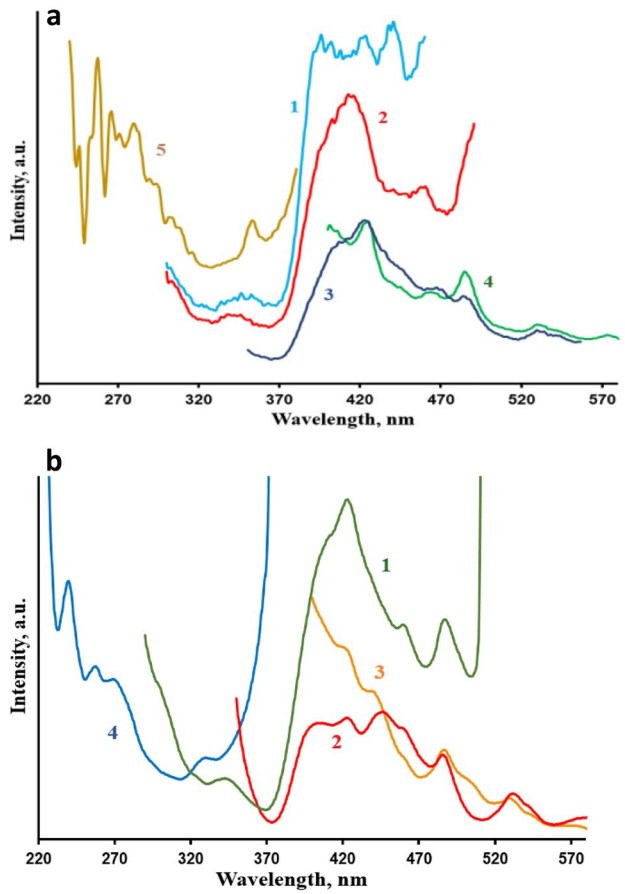

Fig. 3 (**a**) Photoluminescence spectra (curves 1–4) and excitation luminescence spectrum (curve 5) of the sample ***1***. Excitation wavelengths, nm: 240 (curve 1); 257 (curve 2); 272 (curve 3); 330 (curve 4). Emission wavelength, nm: 390 (curve 5). **b** Photoluminescence spectra (curves 1–3) and excitation luminescence spectrum (curve 4) of the sample ***4***. Excitation wavelengths, nm: 270 (curve 1); 330 (curve 2); 370 (curve 3). Emission wavelength, nm: 390 (curve 4)

of carbon–carbon bonds it can destroy different hazardous materials and bacteria and shows a function as sterilization. However, UV-C is very hazardous to organisms [50, 51]. UV-A radiation is friendly to living organisms and is effective in producing tannins and vitamin D [49]. Also, it was reported in [52] that the growth of vegetables plants exposed to UV-A radiation was greater than that of plants exposed to no UV radiation. This effect of UV-A radiation has associated with an increase in chlorophyll content in vegetables and increased photosynthetic activity.

It is worth noticing that some overlapping of the bands in luminescence excitation spectra (curve 5 (Fig. 3a); curve 4 (Fig. 3b)) and emission peaks in luminescence spectra (curves 1 and 2 (Fig. 3a); curve 1 (Fig. 3b) that is observed in the spectral range 330–360 nm. Taking in account this fact and close nanoparticles package in the material structure (Fig. 2) it is possible assuming the possibility of the energy transfer between different centers or to the light reabsorption in composites with the following emission in the visible spectral range.

5 Singlet Oxygen Photogeneration

Figures 4 and 5 show the photoluminescence spectra of prepared powders in near infrared (NIR) spectral range. The luminescent band with $\lambda_{max.} = 1270$ nm which is characteristic for singlet oxygen was observed in photoluminescence spectra of all samples (Figs. 4, 5). The comparison of Figs. 4 and 5 shows that the luminescent band intensities are higher at the irradiation of blue light ($\lambda_{ex} = 405$ nm) (Fig. 5). This is related to the higher power density of blue LED compare with UV LED (see "Material and Methods" section).

6 Antibacterial Activity

Experiments demonstrated antibacterial activity composites against gram-positive bacteria. Figure 6 shows the photo of composite ***1*** disposed inside agar with gram-positive bacteria ***Staphylococcus aureus ATCC 209P***. This photo demonstrates the dark zone surrounding the sample which zone is free from bacteria. The comparison of the thickness of these zones with our previous results [22, 23] shows that prepared nanocomposites demonstrate comparable bactericidal properties against gram-positive with Ag-containing ZnO-based composites.

The mechanisms of antibacterial effect of ZnO-containing nanomaterials include the generation of reactive oxygen species [23, 24, 53, 54], the destruction of bacterial cell integrity [55], diffusion antimicrobial Zn^{2+} ion into the bacterial cell [56]. The obtained experimental results of singlet oxygen photogeneration (Fig. 4) suggest that the generation of reactive oxygen species (ROS) can plays the **key role** in the antibacterial effect of prepared materials.

7 Conclusion

Cu-doped $ZnO/ZnAl_2O_3$ nanocomposites were prepared by polymer-salt synthesis at 680 °C. The nanocomposites consist of small hexagonal ZnO and cubic $ZnAl_2O_4$ nanocrystals having size about 10 nm. The limitation of forming ZnO crystals growth by the chemical conversion of their part into another crystal matrix during material crystallization stage is effective for the synthesis of highly dispersive photoactive materials. Cu ions were embedded into the crystal structure of Zn-containing crystals. Obtained

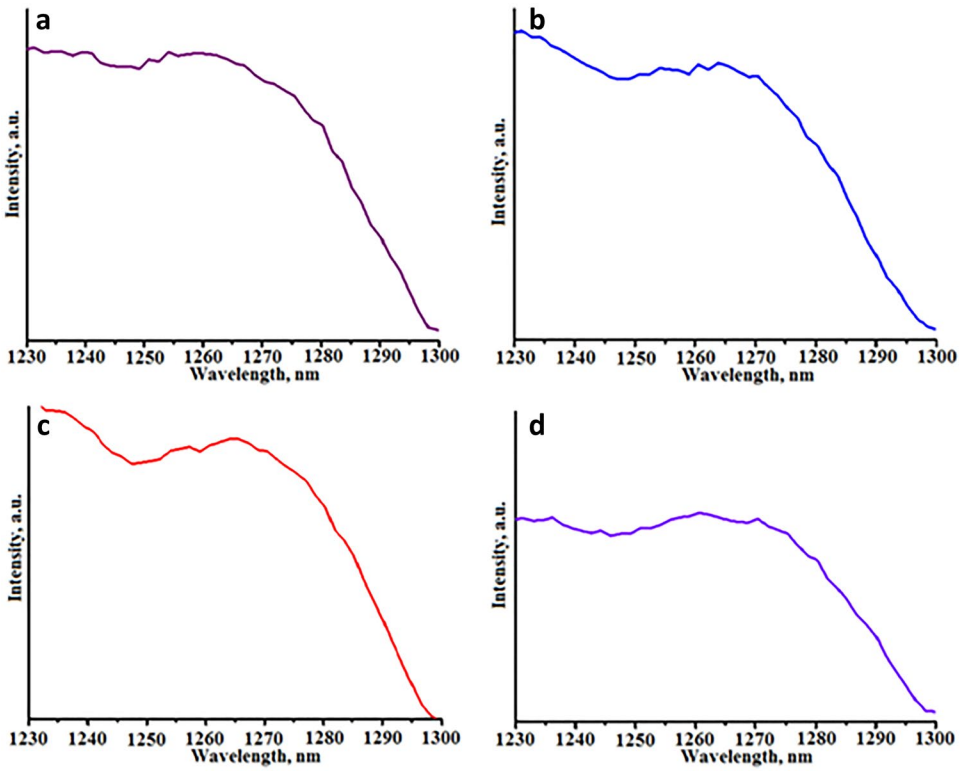

Fig. 4 Photoluminescence spectra ($\lambda_{ex.} = 370$ nm) in near IR spectral range of nanocomposites ***1*** (**a**); ***2*** (**b**); ***3*** (**c**); ***4*** (**d**)

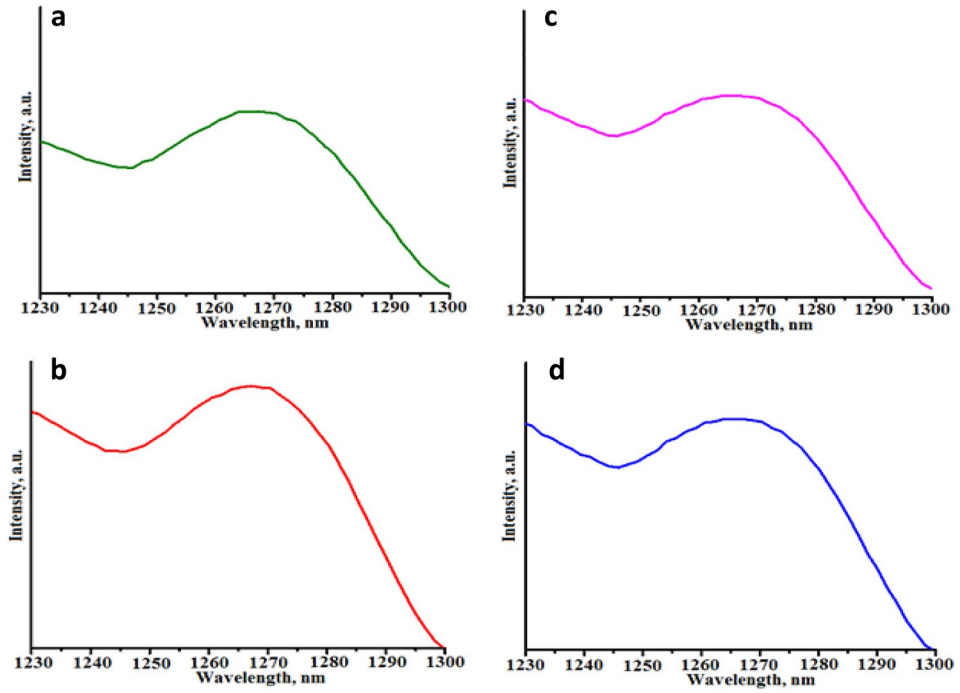

Fig. 5 Photoluminescence spectra ($\lambda_{ex.} = 405$ nm) in near IR spectral range of nanocomposites ***1*** (**a**); ***2*** (**b**); ***3*** (**c**); ***4*** (**d**)

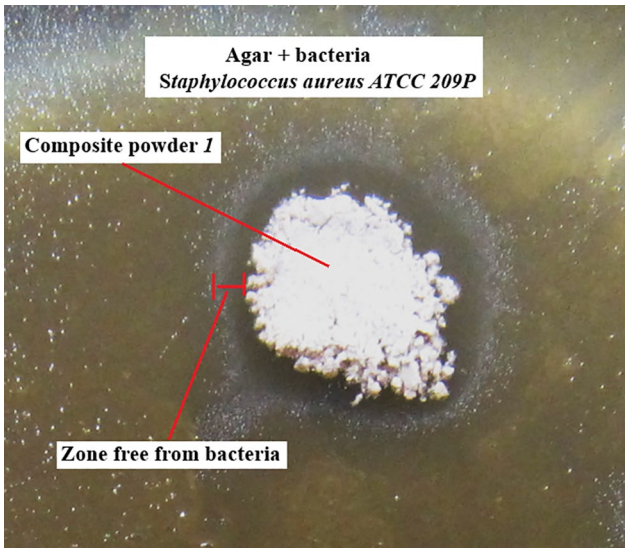

Fig. 6 Photo of composite ***1*** disposed inside agar with gram-positive bacteria ***Staphylococcus aureus ATCC 209P***

nanocomposites can be used as light down-convertors that convert UV-C radiation into UV-A and visible spectral range. Materials demonstrate the ability to generate chemically active singlet oxygen under UV-A radiation and blue light. The experiments show that Cu-doped ZnO–$ZnAl_2O_4$ materials demonstrate antibacterial activity against gram-positive bacteria.

Acknowledgements The reported study was funded by Russian Science Foundation, according to the research project No. 20-19-00559.

Author contributions Tincu and Shelemanov - obtaining data and conducting an experiment Evstropiev - writing the main manuscript text Shelemanov and Evstropiev - preparing figures All authors reviewed the manuscript.

Declarations

Competing interests The authors declare no competing interests.

References

1. B. Allabergenov, U. Shaislamov, H. Shim, M.-J. Lee, A. Matnazarov, B. Choi, Effective control over near band-edge emission in ZnO/CuO multilayred films. Opt. Mater. Express **7**(2), 494–502 (2017)
2. D. Das, P. Mondal, Photoluminescence phenomena prevailing in c-axis oriented intrinsic ZnO thin films prepared by RF magnetron sputtering. RSC Adv. **4**, 35735–35743 (2014). https://doi.org/10.1039/C4RA06063F
3. H. Morkoş, Ü. Özgür, *Zinc Oxide: Fundamentals, Materials and Device Technology*, (Wiley, Weinheim, 2009) ISBN: 978-3-527-40813-9.
4. E.L. Foletto, S. Battiston, J.M. Simões, M.M. Bassaco, L.S.F. Pereira, É.M.M. Flores, E.I. Müller, Synthesis of $ZnAl_2O_4$ nanoparticles by different routes and the effect of its pore size on the photocatalytic process. Microporous Mesoporous Mater. **163**, 29–33 (2012)
5. C.G. Anchieta, D. Sallet, E.L. Foletto, S.S. da Silva, O. Chiavone-Filho, C.A.O. do Nascimento, Synthesis of ternary zinc spinel oxides and their application in the photodegradation of organic pollutant. Ceram. Int. **40**, 4173–4178 (2014). https://doi.org/10.1016/j.ceramint.2013.08.074
6. S. Battiston, C. Rigo, E. Severo, M. Mazutti, R.C. Kuhn, A. Gündel, E.L. Foletto, Synthesis of zinc aluminate ($ZnAl_2O_4$) spinel and its application as photocatalyst. Mater. Res. **17**(3), 734–738 (2014). https://doi.org/10.1590/S1516-14392014005000073
7. M. Zawadzki, W. Staszak, F.E. López-Suárez, M.J. Illán-Gómez, A. Bueno-López, Preparation, characterization and catalytic performance for soot oxidation of copper-containing $ZnAl_2O_4$ spinels. Appl. Catal. A **371**(1–2), 92–98 (2009). https://doi.org/10.1016/j.apcata.2009.09.035
8. L. Cornu, M. Gaudon, V. Jubera, $ZnAl_2O_4$ as a potential sensor: variation of luminescence with thermal history. J. Mater. Chem. C **1**, 5419–5428 (2013). https://doi.org/10.1039/C3TC30964A
9. S.-F. Wang, G.-Z. Sub, L.-M. Fang, L. Lei, X. Xiang, X.-T. Zu, A comparative study of $ZnAl_2O_4$ nanoparticles synthesized from different aluminum salts for use as fluorescence materials. Sci. Rep. **5**, 12849 (2015). https://doi.org/10.1038/srep12849
10. C. Ragupathi, L.J. Kennedy, J.J. Vijaya, A new approach: synthesis, characterization and optical studies of nano-zinc aluminate. Adv. Powder Technol. **25**(1), 267–273 (2014)
11. F.Z. Akika, M. Benamira, H. Lahmar, M. Trari, I. Avramova, Ş Suzer, Structural and optical properties of Cu-doped $ZnAl_2O_4$ and its application as photocatalyst for Cr(VI) reduction under sunlight. Surf. Interfaces **18**, 100406 (2020). https://doi.org/10.1016/j.surfin.2019.100406
12. L. Zhu, H. Li, Z. Liu, P. Xia, Y. Xie, D. Xiong, Synthesis of the 0D/3D CuO/ZnO heterojunction with enhanced photocatalytic activity. J. Phys. Chem. C **122**(17), 9531–9539 (2018). https://doi.org/10.1021/acs.jpcc.8b01933
13. X.-j Guo, L.-M. Li, S.-M. Liu, G.-L. Bao, W.-H. Hou, Preparation of CuO/ZnO/Al_2O_3 catalysts for methanol synthesis using parallel-slurry-mixing method. J. Fuel Chem. Technol. **35**(3), 329–333 (2007). https://doi.org/10.1016/S1872-5813(07)60023-1
14. J. Abu-Dahrich, D. Rooney, A. Goguet, Y. Saih, Activity and deactivation studies for direct dimethyl ether synthesis using CuO-ZnO-Al_2O_3 with NH_4ZSM-5, HZSM-5 or γ-Al_2O_3. Chem. Eng. J. **203**, 201–211 (2012). https://doi.org/10.1016/j.cej.2012.07.011
15. M.A. Subhan, T. Ahmed, R. Awal, R. Makioka, H. Nakata, T.T. Pakkanen, M. Suvanto, B.M. Kim, Synthesis, structure, luminescence and photophysical properties of nano CuO·ZnO·$ZnAl_2O_4$ multi metal oxide. J. Lumin. **146**, 123–127 (2014). https://doi.org/10.1016/j.jlumin.2013.09.045
16. S.V. Motloung, P. Kumari, L.F. Koao, T.E. Motaung, T.T. Hlatshwayo, M.J. Mochane, Effect of annealing time on the structure and optical properties of $ZnAl_2O_4$/ZnO prepared via citrate sol-gel process. Mater. Today Commun. **14**, 294–301 (2018)
17. S. Maslennikov, S. Evstropiev, I. Sochnikov, A. Karavaeva, K. Dukelskii, V. Gridchin, Photoactive UV-A transparent ZnO-Al_2O_3 coatings for singlet oxygen photogeneration. Opt. Engineering **58**(7), 077105 (2019). https://doi.org/10.1117/1.OE.58.7.077105
18. I.S. Boltenkov, E.V. Kolobkova, S.K. Evstropiev, Synthesis and characterization of transparent photocatalytic ZnO-Sm_2O_3 and ZnO-Er_2O_3 coatings. J. Photochem. Photobiol. A **367**, 458–464 (2018). https://doi.org/10.1016/j.photochem.2018.09.016

19. Y.H. Lu, M. Xu, L.X. Xu, C.L. Zhang, Q.P. Zhang, X.N. Xu, S. Xu, K. Ostrikov, Enhanced ultraviolet photocatalytic activity of Ag/ZnO nanoparticles synthesized by modified polymer-network gel method. J. Nanoparticle Res **17**, 350 (2015). https://doi.org/10.1007/s11051-015-3150y
20. M.R. Mhlongo, L.F. Koao, R.E. Kroon, S.V. Motloung, Investigative study of Mn^{2+} concentration on the structure, morphology and luminescence of sol-gel $ZnAl_2O_4$/ZnO/$SrAl_2O_4$/$Sr_3Al_2O_6$ mixed phase nanophosphor. Physica B **578**, 411746 (2020)
21. Y. Li, W. Zhang, J. Niu, Y. Chen, Mechanism of photogenerated reactive oxygen species and correlation with the antibacterial properties of engineered metal-oxide nanoparticles. ACS Nano **6**(6), 5164–5173 (2012)
22. S.K. Evstropiev, A.V. Karavaeva, M.A. Petrova, N.V. Nikonorov, V.N. Vasilyev, L.L. Lesnykh, K.V. Dukelskii, Antibacterial effect of nanostructured ZnO-SnO_2 coatings: the role of microstructure. Mater. Today Commun. **21**, 100628 (2019)
23. A.A. Shelemanov, S.K. Evstropiev, A.V. Karavaeva, N.V. Nikonorov, V.N. Vasilyev, Y.F. Podruhin, V.M. Kiselev, Enhanced singlet oxygen generation by bactericidal ZnO-MgO-Ag nanocomposites. Mater. Chem. Phys. **276**, 125204 (2022). https://doi.org/10.1016/j.matchemphys.2021.125204
24. F. Vatansever, W.C.M.A. de Melo, P. Avci, D. Vecchio, M. Sadasivam, A. Gupta, R. Chandran, M. Karimi, N.A. Parizotto, R. Yin, G.P. Tegos, M.R. Hamblin, Antimicrobial strategy centered around reactive oxygen species—bactericidal antibiotics, photodynamic therapy, and beyond. FEMS Microbiol. Rev. **37**, 955–989 (2013)
25. S.K. Sinha, T. Rakshit, S.K. Ray, I. Manna, Characterization of ZnO-SnO_2 thin film composites prepared by pulsed laser deposition. Appl. Surf. Sci. **257**(1), 10551–10556 (2012)
26. R. Li, L. Zhang, P. Wang, Rational design of nanomaterials for water treatment. Nanoscale **7**, 17167–17194 (2015)
27. K.R. Raghupathi, R.T. Koodali, A.C. Manna, Size-dependent bacterial growth inhibition and mechanism of antibacterial activity of zinc oxide nanoparticles. Langmuir **27**(7), 4040 (2011)
28. K. Qi, B. Cheng, J. Yu, W. Ho, Review on the improvement of the photocatalytic and antibacterial activities of ZnO. J. Alloys Compd. **727**, 792–820 (2017)
29. W.S. Chiu, P.S. Khiew, M. Cloke, D. Isa, T.K. Tan, S. Radiman, R. Abd-Shukor, M.A. Abd. Hamid, N.M. Huang, H.N. Lim, C.H. Chia, Photocatalytic study of two-dimensional ZnO nanopellets in the decomposition of methylene blue. Chem. Eng. J. **158**, 345–352 (2010)
30. S. Wang, P. Kuang, B. Cheng, J. Yu, C. Jiang, ZnO hierarchical microsphere for enhanced photocatalytic activity. J. Alloys Compd. **741**, 622–632 (2018)
31. Z. Cheng, S. Zhao, L. Han, A novel preparation method for ZnO/γ-Al_2O_3 nanofibres with enhanced absorbability and improved photocatalytic water-treatment performance by Ag nanoparticles. Nanoscale **10**, 6892–6899 (2018)
32. R.C. Bradt, S.L. Burkett, Microstructural control of zinc oxide varistor ceramics, in *Ceramic Microstructures: Control at the Atomic Level*. ed. by A.P. Tomsia, A.M. Glaeser (Springer, New York, 1998), pp.339–348
33. J. Theerthagiri, S. Salla, R.A. Senthil, P. Nithyadharseni, A. Madankumar, P. Arunachalam, T. Maiyalagan, H.-S. Kim, A review on ZnO nanostructured materials: energy, environmental and biological applications. Nanotechnology **30**(39), 392001 (2019)
34. F. Lin, B. Cojocaru, C.-L. Chou, C.A. Cadigan, Y. Ji, D. Nordlund, T.-C. Weng, Z. Zheng, V.I. Pârvulescu, R.M. Richards, Photocatalytic activity and selectivity of ZnO materials in the decomposition of organic compounds. ChemCatChem **5**(12), 3841–3846 (2013)
35. X. Zhao, L. Wang, Xu. Xin, X. Lei, Xu. Sailong, F. Zhang, Fabrication and photocatalytic properties of novel ZnO/$ZnAl_2O_4$ nanocomposite with $ZnAl_2O_4$ dispersed inside ZnO network. AIChE J. **58**(2), 573–582 (2012)
36. M. Shahmirzaee, M.S. Afarani, A.M. Arabi, A.I. Nejhad, In situ crystallization of $ZnAl_2O_4$/ZnO nanocomposites on alumina granule for photocatalytic purification of wastewater. Res. Chem. Intermed. **43**, 321–340 (2017). https://doi.org/10.1007/s11164-016-2624-6
37. X. Yuan, X. Cheng, Q. Jing, J. Niu, D. Peng, Z. Feng, X. Wu, ZnO/$ZnAl_2O_4$ nanocomposite with 3D sphere-like hierarchical structure for photocatalytic reduction of aqueous Cr (VI). Materials (Basel) **11**(9), 1624 (2018). https://doi.org/10.3390/ma11091624
38. Li. Zhang, J. Yan, M. Zhou, Y. Yang, Y.-N. Liu, Fabrication and photocatalytic properties of spheres-in-spheres ZnO/$ZnAl_2O_4$ composite hollow microspheres. Appl. Surf. Sci. **268**, 237–245 (2013). https://doi.org/10.1016/j.apsusc.2012.12.069
39. H. Zhao, Y. Dong, P. Jiang, G. Wang, J. Zhang, C. Zhang, $ZnAl_2O_4$ as a novel high-surface-area ozonation catalyst: one-step green synthesis, catalytic performance and mechanism. Chem. Eng. J. **260**, 623–630 (2015). https://doi.org/10.1016/j.cej.2014.09.034
40. A. Chaudhary, A. Mohammad, S.M. Mobin, Facile synthesis of phase pure $ZnAl_2O_4$ nanoparticles for effective photocatalytic degradation of organic dyes. Mater. Sci. Eng. B **227**, 136–144 (2018). https://doi.org/10.1016/j.mseb.2017.10.009
41. S.S. Sampath, D.G. Kanhere, R. Pandey, Electronic structure of spinel oxides: zinc aluminate and zinc gallate. J. Phys: Condens. Matter **11**, 3635–3644 (1999)
42. H. Dixit, N. Tandon, S. Cottenier, R. Saniz, D. Lamoen, B. Partoens, V. Van Speybrock, M. Waroquier, Electronic structure and band gap of zinc oxides beyond LDA: $ZnAl_2O_4$, $ZnGa_2O_4$ and $ZnIn_2O_4$. New J. Phys. **13**, 063002 (2011)
43. T. Tangcharoen, J.T. Thrienprasert, C. Kongmark, Effect of calcination temperature on structural and optical properties of MAl_2O_4 (M=Ni, Cu, Zn) aluminate spinel nanoparticles. J. Adv. Ceram. **8**(3), 352–366 (2019). https://doi.org/10.1007/s40145-019-0317-5
44. Z. Huang, X. Zheng, D. Yan, G. Yin, X. Liao, Y. Kang, Y. Yao, D. Huang, B. Hao, Toxicological effect of ZnO nanoparticles based on bacteria. Langmuir **24**, 4140–4144 (2008)
45. A.A. Shelemanov, R.K. Nuryev, S.K. Evstropiev, V.M. Kiselev, N.V. Nikonorov, The influence of polyvinylpyrrolidone on the structure and optical properties of ZnO-MgO nanocomposites synthesized by the polymer-salt method. Opt. Spectr. **129**(9), 1176–1181 (2021)
46. A.R. Lim, Effects of paramagnetic interactions by the partial replacement of Zn^{2+} ions with Cu^{2+} ions in lead-free zinc-based perovskite $(MA)_2ZnCl_4$ crystal by MAS NMR. AIP Adv. **9**, 105115 (2019). https://doi.org/10.1063/1.5121443
47. F. Davar, M. Salavati-Niasari, Synthesis and characterization of spinel-type zinc aluminate nanoparticles by a modified sol-gel method using new precursor. J. Alloys Compd. **509**(5), 2487–2492 (2011). https://doi.org/10.1016/j.jallcom.2010.11.058
48. P.A. Rodnyi, K.A. Chernenko, I.D. Venevtsev, Mechnaisms of ZnO luminescence in the visible spectral region. Opt. Spectr. **125**(3), 372–378 (2018). https://doi.org/10.1134/S0030400X18090205
49. H. Komitami, N. Sonoda, K. Hara, Preparation and luminescent characteristics of UV-C emitting $ZnAl_2O_4$ phosphor for sterilization device, in *Proceedings of the International Display Workshops, IDW'20*, (2020) p. 346–349.
50. F. Hollósy, Effect of ultraviolet radiation on plant cells. Micron **33**(2), 179–197 (2002). https://doi.org/10.1016/s0968-4328(01)00011-7

51. B.B. Surjadinata, D.A. Jacobo-Velázquez, L. Cisneros-Zevallos, UVA, UVB and UVC light enhances the biosynthesis of phenolic antioxidants in fresh-cut carrot through a synergistic effect with wounding. Molecules **22**(4), 668 (2017). https://doi.org/10.3390/molecules22040668
52. T. Tezuka, T. Hotta, I. Watanabe, Growth promotion of tomato and radish plants by solar UV radiation reaching the Earth's surface. J. Photochem. Phobiol. B **19**(1), 3061–3066 (1999)
53. A. Sirelkhatim, S. Mahmud, A. Seeni, N.H.M. Kaus, L.C. Ann, S.K.M. Bakhori, H. Hasan, D. Mohamad, Review of zinc oxide nanoparticles: antibacterial activity and toxicity mechanism. Nano-Micro Lett. **7**(3), 219–242 (2015). https://doi.org/10.1007/s40820-015-0040-x
54. L. Zhang, Y. Ding, M. Povey, D. York, ZnO nanofluids—a potential antibacterial agent. Prog. Nat. Sci. **18**(8), 939–944 (2008)
55. L.K. Adams, D.Y. Lyon, P.J. Alvarez, Comparative eco-toxicity of nanoscale TiO_2, SiO_2 and ZnO water suspensions. Water Res. **40**(19), 3527–3532 (2006)
56. M. Li, L. Zhu, D. Lin, Toxicity of ZnO nanoparticles to *Escherichia coli*: mechanism and the influence of medium components. Environ. Sci. Technol. **45**(5), 1977–1983 (2011)